Effect of Selenium on the Interaction Between Refractory and Steel

LIMEI CHENG, WEN YANG, YING REN, and LIFENG ZHANG

The presence of surface-active selenium in liquid steel has an obvious effect on the wettability between steel and inclusions, significantly affecting inclusion behaviors in liquid steel. In the current study, the influence of surfactant on the interaction between the refractory and liquid iron was investigated. The contact angles between the refractory and liquid iron with and without the selenium addition were measured using the sessile drop method at 1873 K. Besides, the interfacial reaction layer between the iron and refractory was investigated using scanning electron microscopy. It was found that the addition of selenium increased the contact angle between the iron and the refractory and affected the penetration behavior of liquid iron into the refractory.

https://doi.org/10.1007/s11663-019-01545-9
© The Minerals, Metals & Materials Society and ASM International 2019

I. INTRODUCTION

REFRACTORIES are widely used in the steel industry, such as the blast furnace lining, steel ladle lining, and tundish lining,[1] due to its high corrosion resistance, low thermal expansion, and good thermal conductivity. In the steel production process, the refractory as the vessel lining material directly contacts with the molten steel. The interaction between the refractory and steel has a significant influence on the service life of the ladle lining, the steel quality,[2,3] and the production safety. The corrosion resistance to the molten steel is one of the major issues for the production of the high-quality steel. Recently, with the increase of demands for the advanced refractory in the metallurgical industry, more and more attention is focused on the interaction between the refractory and steel.[4–11] Huang *et al.*[9] investigated the effect of the alumina-magnesia refractories and the molten steel interaction on the steel cleanliness during the smelting process. It was indicated that alumina-magnesia carbon-free castable can be used as the lining material for the production of high-quality alloy steel. Wei *et al.*[10] studied the reaction mechanism of the alumina carbon refractory and Fe system by the thermal gravity experiment with different temperatures and soaking times. It was concluded that carbonaceous materials played a key role in the interaction of the refractory and steel. The presence of refractory in iron was mainly caused by the carbothermic reduction of Al_2O_3 and carbonaceous materials, instead of the dissolution of Al_2O_3 in iron. Fruhstorfer *et al.*[11] investigated the corrosion of alumina refractory by alloyed steels. It was proposed that interactions between the steel alloy and the refractory can increase the corrosivity of steel.

The interaction between steel and refractory is mainly caused by the chemical reaction and the molten metal penetration. The interfacial phenomenon at the refractory/steel interface has a huge influence on the microstructure evolution of the contact area of the solid refractory material and the molten steel. Zhukovskaya *et al.*[12] proved that the molten iron penetration depth into the refractory was closely related to the wettability between the molten steel and the refractory, which was usually represented as the contact angle. Therefore, it is meaningful to investigate the wetting behavior between the molten steel and the refractory to improve their interaction. Ogino and co-workers[13,14] reviewed the contact angle between the alumina substrate and the molten steel containing the surface-active elements, such as oxygen, sulfur, selenium, or tellurium. However, the effect of wettability on the interaction between the refractory and the molten steel was neglected.

As a surface-active element, selenium is widely used as an additive in steel to improve machinability in the steel production.[15,16] However, most of the previous studies on the effect of selenium in steel mainly focused on the inclusion behavior[17–19] and surface segregation.[20,21] The effect of selenium on the interaction of steel and refractory was rarely reported. In the current study, the effect of the surface-active element selenium on the interaction between the refractory and the steel was

LIMEI CHENG, WEN YANG, YING REN, and LIFENG ZHANG are with the School of Metallurgical and Ecological Engineering, University of Science and Technology Beijing (USTB), Beijing 100083, China. Contact emails: renyingfour@163.com, zhanglifeng@ustb.edu.cn

Manuscript submitted October 31, 2018.
Article published online March 15, 2019.

investigated through laboratory experiments. The selenium was added in the liquid iron to change the interfacial properties of the refractory and the liquid iron.

II. EXPERIMENTAL PROCEDURE

In the current study, the measurement schematic of the wettability between the iron and an alumina-magnesia substrate using the sessile drop apparatus is shown in Figure 1. The used contact angle device is DataPhysics OCA 20, made in Germany. The alumina-magnesia substrates were prepared by pressing a mixture of pure MgO and pure Al_2O_3 powders with the molar ratio of 1:1 into a thin substrate with 3-mm height and 30-mm diameter under a pressure of 20 tons, and then they were sintered for 2 hours at 1873 K in air. Also, the surface of the sintered substrate was polished by abrasive paper and diamond paste. In order to prevent small particles in the refractory from falling off, the polishing rotational speed was chosen to have a relatively slow value of 150 rev/min. The iron sample was cut into a cylinder with 5.5-mm height and 3-mm diameter to ensure the formation of the forward contact angle during the experiment. And then the iron sample was polished to remove impurities on the sample surface and cleaned in ethanol by using an ultrasonic cleaner. Based on our previous study,[8] when the Al content in iron was over 300 ppm, there was an obvious interfacial reaction of the iron sample and magnesia refractory. The formation of magnesia-alumina spinel on the iron sample surface obviously influenced the accuracy of the contact angle measurement. Therefore, the Al content in the iron sample was controlled as 250 ppm in current experiments. The detailed experimental conditions and oxygen partial pressures are listed in Tables I and II, respectively. First, the iron sample was placed in the center of the alumina-magnesia refractory substrate, which was supported by an alumina plate. Then, the standard accessory for placing sample was used to put the assembly in the same position in the constant temperature zone of the high-temperature contact angle device, and the temperature of the constant temperature zone was calibrated by a special standard thermocouple. The assembly was heated from room temperature to the desired temperature of 1873 K at a heating rate of 5 °C/min and held for 40 minutes. The experiment was conducted under a reducing atmosphere of Ar mixed with 10 pct H_2 in volume fraction. For the high-temperature contact angle device, both sides of the alumina tube were sealed by flange plates and the terminal was fixed with quartz glass. During the experiment, the image of the sample was recorded by a CCD camera at a frame rate of 20 frames per minute, and the drop profile can be marked by the software SCA 20 using the Young–Laplace fitting to automatically calculate the contact angle between the iron and the refractory after setting up the demarcation line between the iron and refractory.

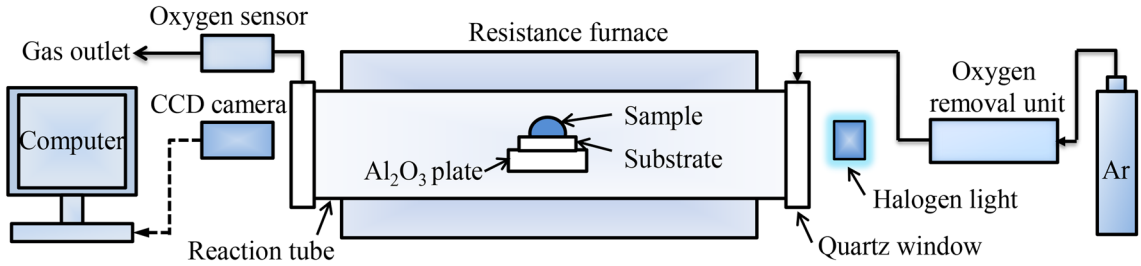

Fig. 1—Schematic of the sessile drop apparatus.

Table I. Composition, Size, and Weight of the Iron Samples

Number	Substrate	Iron		Atmosphere	Holding Time (1873 K)	Size (mm)	Weight (g)
		Se (ppm)	Al (ppm)				
1	50 pct Al_2O_3 + 50 pct MgO	0	250	Ar + 10 pct H_2	40 min	Φ 3 × 5.5	0.1465
2	50 pct Al_2O_3 + 50 pct MgO	250	250	Ar + 10 pct H_2	40 min	Φ 3 × 5	0.1315

Table II. Experimental Oxygen Partial Pressures

Number	Oxygen Partial Pressures (ppm) (Measured at 1023 K)	Oxygen Partial Pressures (ppm) (Calculated at 1823 K)
1	8.8×10^{-20} to 1.5×10^{-19}	9.8×10^{-9} to 1.7×10^{-8}
2	7.9×10^{-20} to 1.9×10^{-19}	8.8×10^{-9} to 2.1×10^{-8}

III. RESULTS AND DISCUSSION

A. *Contact Angle Measurement Results*

The contact angle (θ) reflects wetting behaviors between the liquid iron and the refractory. It is defined as "wetting" at contact angles less than 90 deg and "nonwetting" at contact angles more than 90 deg. As shown in Figure 2, the iron samples with and without the addition of selenium were both nonwetting on alumina-magnesia refractory substrates. They kept their original spherical shape with the average apparent contact angles of 133.5 and 142.6 deg, respectively. The selenium addition in iron increases the measured contact angle.

Figure 3 shows the measured contact angles between the refractory substrate and the liquid iron with and without the addition of selenium. In our previous study, it was concluded that the contact angle between the liquid iron and the alumina-magnesia refractory picked up with an increase of the alumina content in the iron.[8] The dissolved oxygen decreased with the increase of Al content in steel with the same T.O. content, leading to the increase of the contact angle.[13,14] As shown in Figure 3(a), the measured contact angle was compared with the results reported in the literature. The contact angles were all very stable at both the temperature rising stage and the constant temperature stage. As selenium was added in iron, the initial contact angle increased from 134.7 to 144.1 deg, indicating that the selenium addition obviously affected the contact angle between the liquid iron and the refractory. In Figure 3(b), the variation of the contact angle between the alumina-magnesia refractory and the liquid iron with the selenium addition was similar to that between the liquid iron and the alumina refractory,[13,14] indicating that the effect of selenium addition on the contact angle between iron and various refractories was similar.

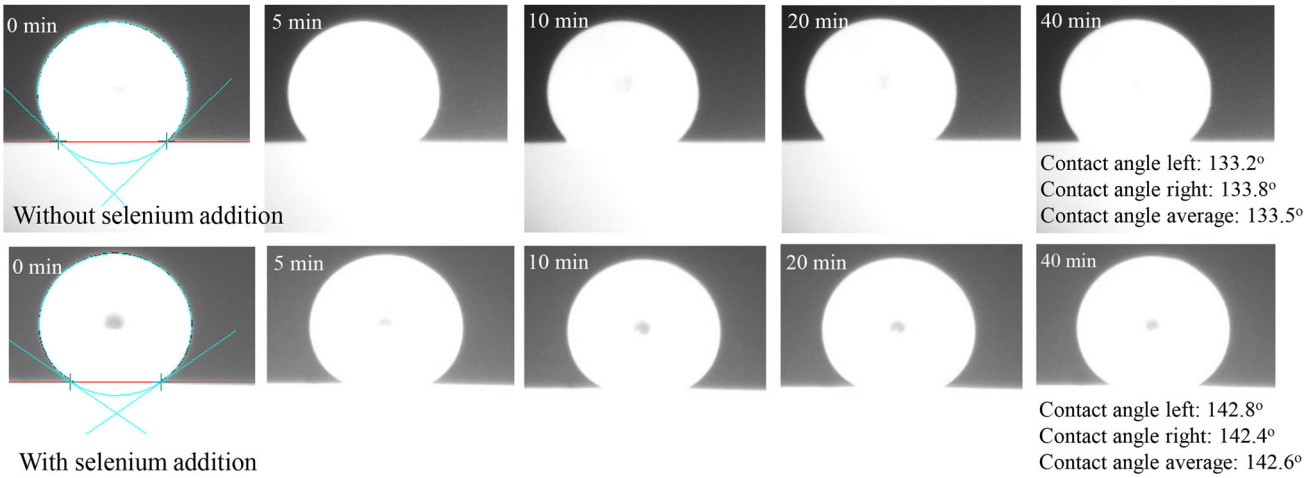

Fig. 2—Morphological variations of liquid iron with and without the addition of selenium on alumina-magnesia substrates at 1873 K.

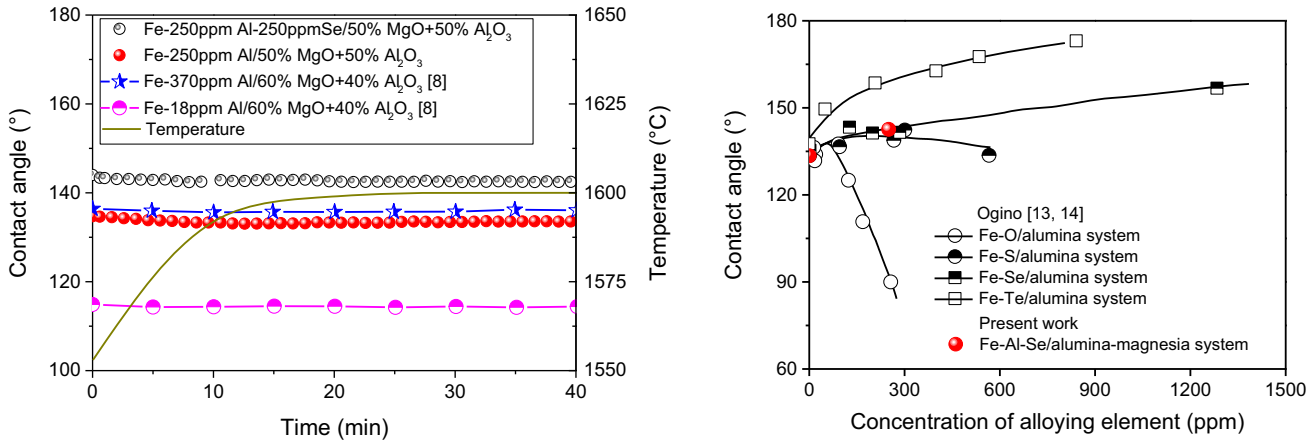

(a) Variation with time

(b) Variation with selenium content

Fig. 3—Variation of the contact angle between liquid iron with and without the addition of selenium on refractory substrates: (*a*) variation with time and (*b*) variation with selenium content.

B. *Effect of Surface-Active Element on the Contact Angle between Iron and Refractory*

The interfacial tension of the liquid iron with the surface-active element and the refractory can be described by the Belton equation,[22] which is a combination of Gibbs and Langmuir adsorption isotherms, as shown in Eq. [1]. When surface-active element was added into iron, the dissolved surface-active element segregated to a surface site in order to occupy a vacant site on the metal surface, as shown in Figure 4. It is described by the following reaction in Eq. [2]. Thus, on the condition of single site occupancy, the equilibrium constant K can be defined as Eq. [3]. Considering the effect of temperature on the surface tension of the pure metal, the surface tension of iron-solute (i) alloys can be obtained from the following Eq. [4].[22]

$$\gamma^0 - \gamma = \mathrm{R}T\Gamma_\mathrm{s} \ln(1 + Ka_i) \quad [1]$$

$$\underline{i} + v^\mathrm{s} = i^\mathrm{s} \quad [2]$$

$$K = e^{-(\Delta G^0/\mathrm{R}T)} = \mathrm{k}_1 e^{-(\Delta H^0/\mathrm{R}T)} \quad [3]$$

$$\gamma_\mathrm{lg} = \gamma_\mathrm{m}^0 - A(T - T_\mathrm{m}) - \mathrm{R}T\Gamma_\mathrm{s} \ln\left(1 + \mathrm{k}_1 a_i e^{-(\Delta H^0/\mathrm{R}T)}\right) \quad [4]$$

where γ^0 and γ are the interfacial tension without and with the surface-active elements, N/m; γ_{lg} is the surface tension of iron, N/m; γ_m^0 is the surface tension of the pure iron at the melting point, N/m; Γ_s is the surface excess at saturation, mol/cm^2; K is the adsorption coefficient; a_i is the activity of species i in solution; $\underline{i}$ is the dissolved species I; R is the gas constant, J/(mol K); v^s is a vacant site on the metal surface; i^s is a site occupied by species i; ΔG^0 is the Gibbs free energy for Eq. [2], J/mol; k_1 is a constant relating to the entropy of Eq. [2]; ΔH^0 is the standard heat of the adsorption, J/mol; and A is the negative of $d\gamma/dT$ for the pure iron, N/(m K).

Specially, the surface tension in the Fe-Se system was investigated by Ogino *et al.*[13] and Sahoo *et al.*,[22] γ_m^0 is 1.843 N/m at 1823 K, the surface excess of selenium Γ_Se is 12.8 × 10^{10} mol/cm^2, A is 4.3 × 10^{-4} N/(m K), ΔH^0 is − 1.098 × 10^5 J/mol, and k_1 is 0.857. It is assumed that the activity of selenium is the selenium content in iron.[22]

Figure 5 shows the basic geometry of a liquid iron drop on a smooth solid surface. In Figure 5(a), γ_{sl} is the interfacial tension between the liquid and the solid surfaces and γ_{sg} is the surface tension of the solid surface. The radius of the liquid iron drop is denoted by r, and the radius of the three-phase contact line is r_1. The geometry can be shown in Eq. [5]. Using a spherical cap model,[23] the droplet volume V is calculated, as shown in Eq. [6]. In order to calculate the total energy conservation of the liquid drop system, the areas of the cap and liquid-solid interfaces can be obtained as follows in Eqs. [7] and [8].

$$r_1 = r \sin\theta \quad [5]$$

$$V = \frac{\pi}{3} r^3 \left(2 - 3\cos\theta + \cos^3\theta\right) \quad [6]$$

$$A_\mathrm{lg} = 2\pi r^2 (1 - \cos\theta) \quad [7]$$

$$A_\mathrm{sl} = \pi r_1^2 = \pi r^2 \sin^2\theta \quad [8]$$

where θ is the contact angle between the molten iron and the solid substrate, larger than 90 deg due to the nonwetted property, deg; r is the radius of the liquid iron drop, meters; r_1 is the radius of the three-phase contact line, meters; V is the volume of the liquid drop, m^3; A_lg is the area of the liquid cap, m^2; and A_sl is the area of the liquid-solid interfaces, m^2.

When a liquid drop is stationary on a surface, the total energy of the liquid drop system is considered to include three parts. First is the free surface energy of the liquid (E_1), as shown in Eq. [9]. The second part is the free surface energy of the area between the liquid and

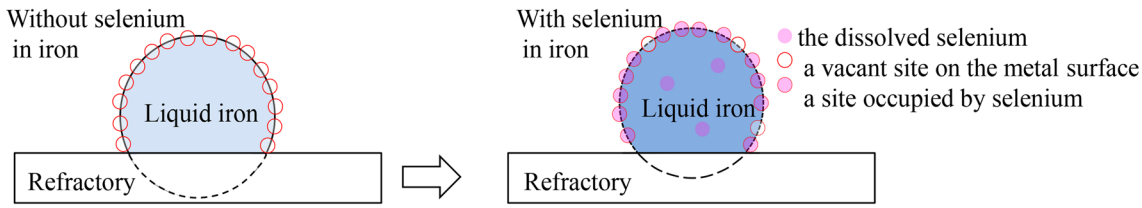

Fig. 4—Effect of selenium in iron on the iron surface.

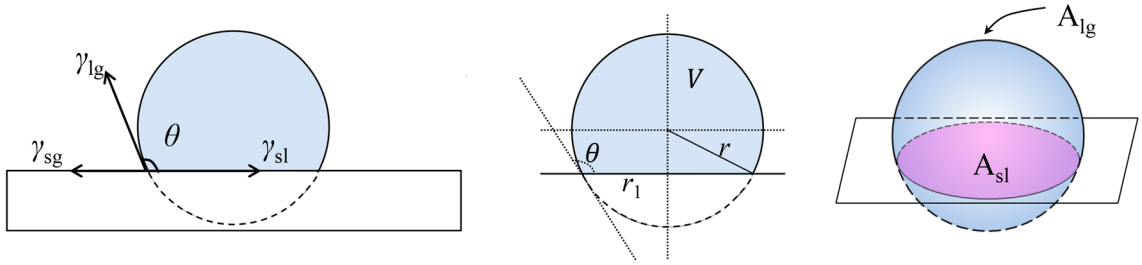

(a) Force balance along the x axis

(b) Two-dimensional geometry of a drop on a surface

(c) Three-dimensional geometry of a drop on a surface

Fig. 5—Geometrical illustration of the cavity between two isodiametric spherical inclusions in molten steel: (*a*) force balance along the *x*-axis, (*b*) two-dimensional geometry of a drop on a surface, and (*c*) three-dimensional geometry of a drop on a surface.

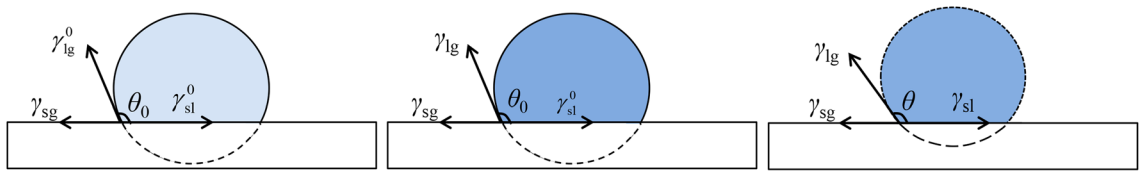

Case 0: before Se addition

Case 1: immediately after Se addition

Case 2: after reaching stable

Fig. 6—Effect of selenium on the wettability of iron and refractory.

the surface (E_2), as shown in Eq. [10]. The last part is the vapor energy (E_3), as given in Eq. [11]. The effect of gravity is ignored since the liquid drop is small enough. Thus, the total free energy of the system (E) is expressed as Eq. [12]:

$$E_l = A_{lg}\gamma_{lg} \quad [9]$$

$$E_2 = (\gamma_{sl} - \gamma_{sg})A_{sl} \quad [10]$$

$$E_3 = \Delta pV \quad [11]$$

$$E = A_{lg}\gamma_{lg} + (\gamma_{sl} - \gamma_{sg})A_{sl} + \Delta pV \quad [12]$$

where E_1 is the free surface energy of the liquid, Joules; E_2 is the free surface energy of the area between the liquid and the surface, Joules; E_3 is the vapor energy, Joules; E is the total free energy of the system, Joules; γ_{sl} is the interfacial tension between the liquid and the solid surface, N/m; γ_{sg} is the surface tension of the solid surface, N/m; and Δp is the pressure deficiency across the meniscus, Pascals.

Figure 6 shows the effect of selenium on the wettability of iron and refractory. In case 0, there is no selenium addition in the iron and the liquid drop is stable. The radius of the liquid drop is r_0; the contact angle is θ_0; and the surface tension and interfacial tension are γ_{lg}^0 and γ_{sl}^0, respectively. In the current experiments, every experimental condition is the same. Also, the atmosphere pressure is about 1 bar pressure. It is reported that the partial pressure of selenium is at parts per million level with a parts per million level selenium in iron.[24] Compared with the atmosphere pressure, it has little effect on the pressure. Thus, the pressure deficiency across the meniscus is assumed to be constant. The addition of selenium can hardly lead to an obvious change in the atmospheric pressure of 1 bar. Thus, it is assumed that the pressure deficiency across the meniscus is a constant. Then, the shape of the liquid drop is unchanged. The interfacial tension and contact angle are still γ_{sl}^0 and θ_0, and the surface tension is γ_{lg}. At that moment, the forces along the horizontal axis are in an unsteady state, leading to the change of the shape of the liquid drop. When the system reaches a new force balance in case 2, the interfacial tension and the contact angle change to γ_{lg} and θ, respectively, and the radius of the liquid drop is r.

Based on the experimental results, the contact angle between the pure iron and the refractory changes little with time. It is assumed that the selenium has little effect on the iron density. Adding selenium in the iron sample can hardly change the mass of the iron sample in each case. Then, the droplet volume is constant. Thus, Eq. [13] is obtained from Eq. [6]. Equation [14] is based on the energy conservation. Equations [15] and [16] are obtained according to Eq. [12]. On the basis of the Young equation, the force balances for cases 0 and 2 are expressed in Eqs. [17] and [18], respectively. Substituting Eqs. [7] and [8] and Eqs. [15] through [18] into Eqs. [14] and [19] can be deduced.

$$\frac{\pi}{3}r^3(2 - 3\cos\theta + \cos^3\theta) = \frac{\pi}{3}r_0^3(2 - 3\cos\theta_0 + \cos^3\theta_0) \quad [13]$$

$$E_{\text{Case1}} = E_{\text{Case2}} \quad [14]$$

$$E_{\text{Case1}} = A_{\text{lg}}^{0}\gamma_{\text{lg}} + \left(\gamma_{\text{sl}}^{0} - \gamma_{\text{sg}}\right)A_{\text{sl}}^{0} + \Delta pV \quad [15]$$

$$E_{\text{Case2}} = A_{\text{lg}}\gamma_{\text{lg}} + \left(\gamma_{\text{sl}} - \gamma_{\text{sg}}\right)A_{\text{sl}} + \Delta pV \quad [16]$$

$$\gamma_{\text{lg}}^{0}\cos\theta_0 + \gamma_{\text{sl}}^{0} - \gamma_{\text{sg}} = 0 \quad [17]$$

$$\gamma_{\text{lg}}\cos\theta + \gamma_{\text{sl}} - \gamma_{\text{sg}} = 0 \quad [18]$$

$$\left(\frac{r}{r_0}\right)^2 = \frac{2\gamma_{\text{lg}}(1-\cos\theta_0) - \gamma_{\text{lg}}^{0}\cos\theta_0\sin^2\theta_0}{2\gamma_{\text{lg}}(1-\cos\theta) - \gamma_{\text{lg}}\cos\theta\sin^2\theta} \quad [19]$$

where $E_{\text{Case 1}}$ and $E_{\text{Case 2}}$ are the total free energy of the system Cases 1 and 2, Joules.

Coupling Eqs. [13] and [19], the variation of the contact angle with the surface tension affected by the selenium addition in iron can be calculated. Then, the calculated relationship between the initial contact angle and selenium content in iron is shown in Figure 7. In order to validate the calculation model, first, the effect of selenium on the Fe/Al_2O_3 system is calculated, as shown by the solid line in Figure 7, which is in good agreement with the measured results obtained from Ogino,[13,14] indicating that the current calculation can be used to predict the wettability between Fe-Se alloy and refractory. Further, based on the calculation model, the variation of the contact angle between the iron containing 250 ppm Al and the alumina-magnesia refractory with selenium in iron is obtained, as shown by the dashed line in Figure 7, which agrees well with the current measured results.

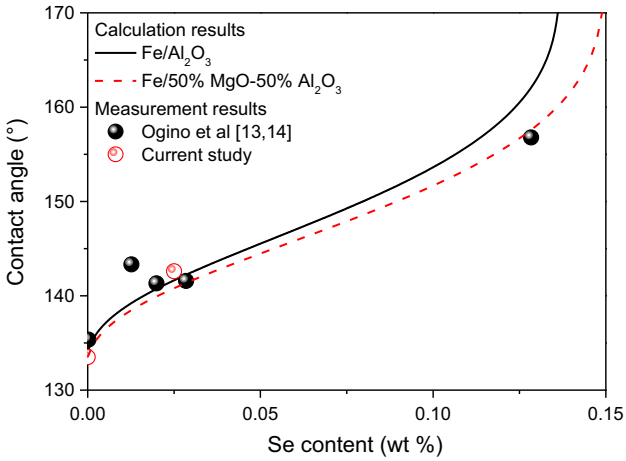

Fig. 7—Variation of contact angle with the selenium addition.

C. *Effect of Selenium Addition on the Penetration of the Liquid Iron into the Refractory Substrate*

Figure 8 shows the cross-sectional morphology of samples after the contact angle measurement experiments obtained by scanning electron microscopy (SEM). Figure 8(a) is the schematic diagram of the analyzed areas using SEM. As shown in Figure 8(b), the small white spots in the refractory were the iron particles, which existed in the whole refractory. The iron particles away from the iron and refractory interface showed a relatively uniform distribution, which was caused by impurity. On the other hand, more iron particles were gathered close to the iron and refractory interface, which should come from the penetration of the liquid iron drop through the pores in the iron and refractory interface. According to the previous study, when the liquid phase in the substrate was formed, it filled in most of the pores and prevented the further penetration of the liquid iron.[8] In order to investigate the influence of selenium on the iron penetration in the refractory, the penetration depth of the liquid iron in each area was measured. For the penetration depth measurement, the iron particle enrichment region was chosen to measure the maximum distance between the iron particle and iron/refractory interface. Also, in order to improve the measurement precision, multiple measurements at many fields using SEM were averaged.

Figure 9(a) is a schematic of the penetration depth measurement. More than ten pictures for the interface of the iron and refractory substrate were obtained using SEM. In each picture, the maximum iron penetration depth was measured and defined as the depth of the iron penetration. The average measurement results are shown in Figure 9(b). The average penetration depth of the iron without selenium into the refractory was 96 μm. With the addition of selenium in iron, the average penetration depth of the liquid iron was reduced to approximately 80 μm.

It can be seen from Figure 8(b) that there were many pores in the substrate in the micron scale. As reported in previous studies,[25–28] the liquid drop on the porous media would go into the pores because of the gravity (F_G), the Laplace pressure force (F_D), and the surface tension (F_M) of a meniscus in a pore. The gravity and the Laplace pressure force were always downward, promoting the liquid penetration, while the direction of the meniscus was determined by the angle (θ_m) between the meniscus and the pore. The three forces can be calculated by Eqs. [20] through [22],[25] and the balance force F is expressed as in Eq. [23].

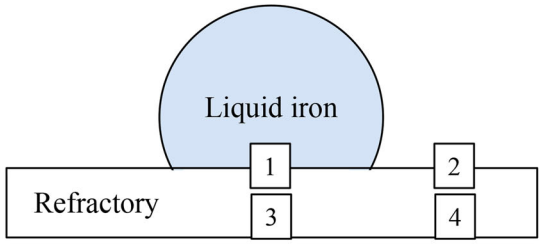

(a) Schematic diagram of the cross section

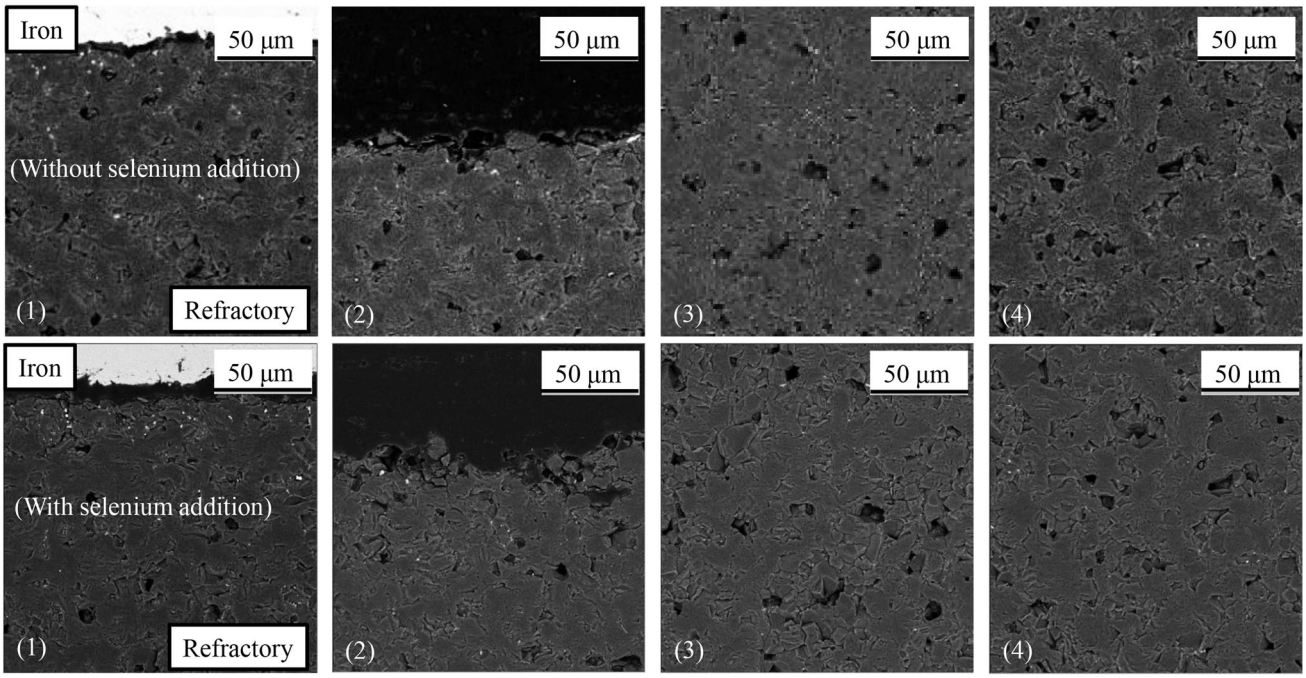

(b) Cross section of the substrate in different areas

Fig. 8—Cross section of samples after experiment: (*a*) schematic diagram of the cross section and (*b*) cross section of the substrate in different areas.

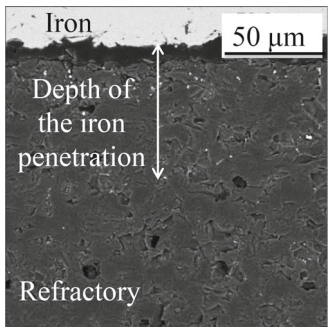

(a) Schematic of the penetration depth measurement

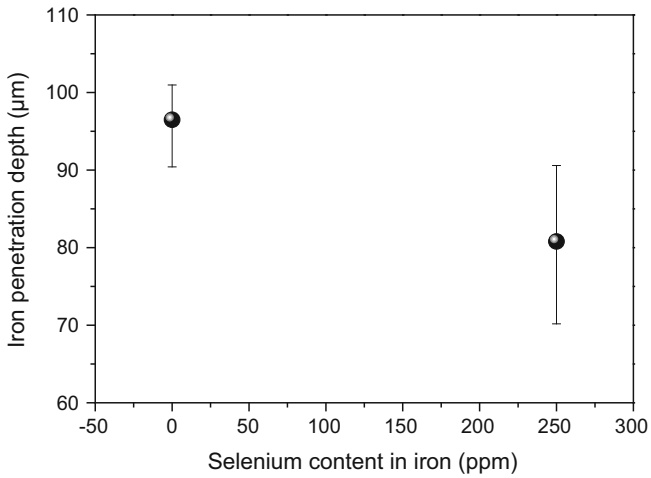

(b) Measured average penetration depth of iron

Fig. 9—Iron penetration depth into the refractory: (*a*) schematic of the penetration depth measurement and (*b*) measured average penetration depth of iron.

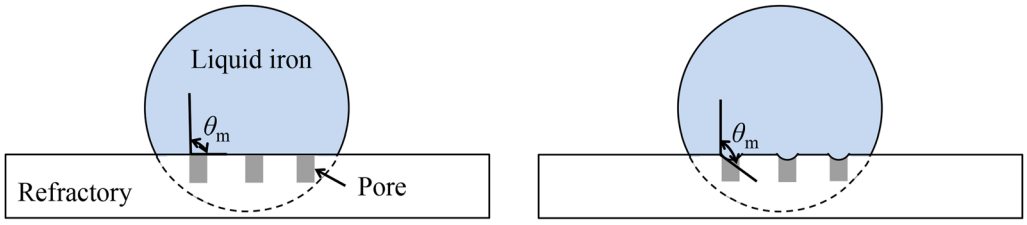

(a) Initial time **(b)** Final moment

Fig. 10—Schematics of a liquid iron drop on the refractory surface: (*a*) initial time and (*b*) final moment.

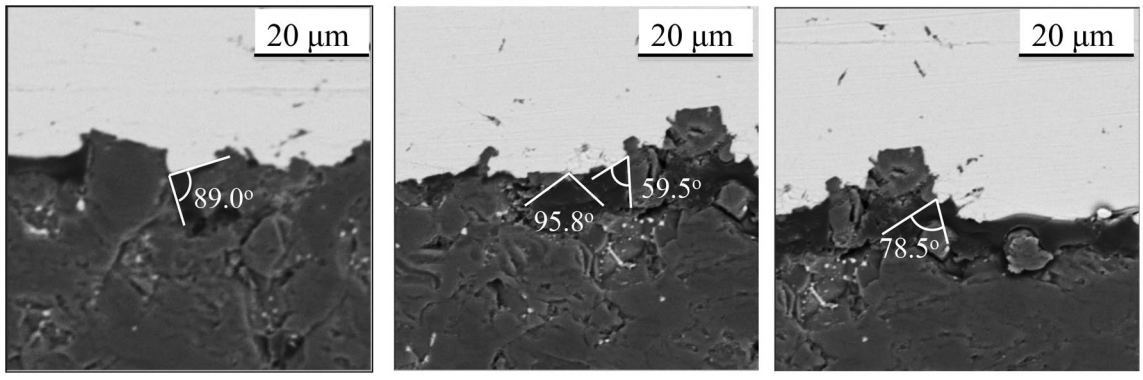

(a) Without selenium addition

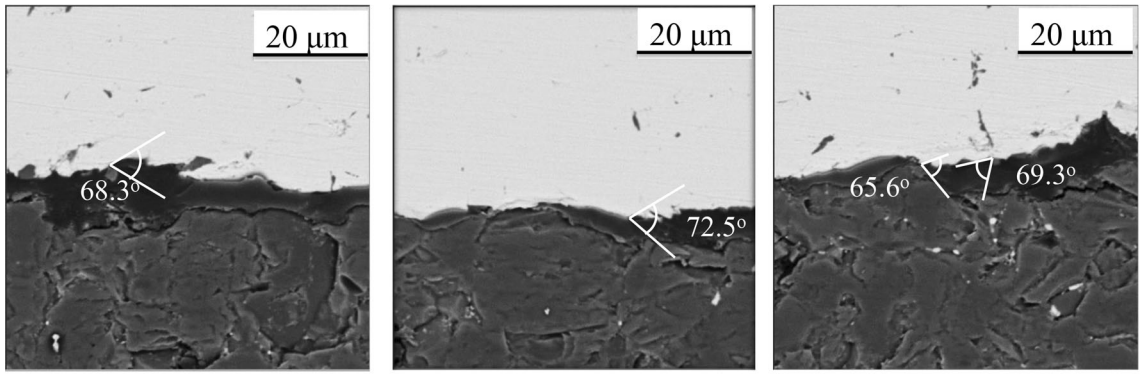

(b) With selenium addition

Fig. 11—Measurement of the angles between the meniscus and the pore: (*a*) without selenium addition and (*b*) with selenium addition.

$$F_{\mathrm{G}} = \rho g r (1 - \cos\theta)\frac{\pi d^2}{4} \quad [20]$$

$$F_{\mathrm{D}} = \frac{\pi \gamma_{\mathrm{lg}} d^2}{2r} \quad [21]$$

$$F_{\mathrm{M}} = \pi d \gamma_{\mathrm{lg}} \cos\theta_{\mathrm{m}} \quad [22]$$

$$\begin{aligned} F &= F_D + F_G + F_M \\ &= \frac{\pi \gamma_{\mathrm{lg}} d^2}{2r} + \rho g r (1 - \cos\theta)\frac{\pi d^2}{4} + \pi d \gamma_{\mathrm{lg}} \cos\theta_m \end{aligned} \quad [23]$$

where F_G is the gravity, Newtons; F_D is the Laplace pressure force, Newtons; F_M is the surface tension of a meniscus in a pore, Newtons; d is the pore size, meters; and θ_m is the angle between the meniscus and the pore, deg.

On the basis of Eq. [22], when the θ_m is larger than 90 deg, the force F_M is less than 0. This means that the surface force F_M is in the upward direction, preventing the penetration of the liquid iron in the pores. As shown in Figure 10, at the initial time after melting of the iron sample, the θ_m is equal to 90 deg, leading to $F_M = 0$. At the final time of the experiment, the θ_m is larger than 90 deg due to the nonwetting between the iron and the refractory, which is measured using SEM, as shown in Figure 11. Table III presents the measured results. There was no obvious interfacial reaction layer observed between the iron and the refractory, as shown in

Table III. Measurement Results of the Angles Between the Meniscus and the Pore

	Without Selenium Addition					With Selenium Addition				
Number	1	2	3	4	Average	1	2	3	4	Average
Measured Angle (deg)	89.0	95.8	59.5	78.5	80.7	68.3	72.5	70.7	65.6	69.3
Meniscus Angle (deg)	91	110.4	115.7	101.5	99.3	111.7	107.5	110.3	114.4	110.7

Figure 8(b). In Figures 2 and 3(a), the contact angle hardly changed with time, indicating that the interfacial reaction had little effect on the change of interfacial geometry. Therefore, the influence of interfacial reaction kinetics on θ_m was not considered. After the selenium addition, the meniscus angle increases from 99.3 to 110.7 deg, the radius of iron drop decreases from 4.3 to 3.8 μm, and the surface tension calculated by Eq. [4] at 1873 K decreases from 1.82 to 1.15 N/m. It is assumed that the pore size for the two experiments is 10 μm according to the measured average size. Based on Eq. [21], after adding selenium, the calculated balance force F decreases from 1.06×10^{-6} N to 8.53×10^{-8} N at the initial time after melting and from -8.98×10^{-6} N to -1.26×10^{-5} N at the final time. This finding indicates that the selenium addition can prevent the iron penetration, which is consistent with the experimental results.

IV. CONCLUSIONS

In the current study, laboratory experiments were performed to investigate the effect of the addition of selenium in iron on the interaction between refractory and steel. The following conclusions were obtained.

1. In the current experimental condition, the addition of selenium increased the contact angle between molten steel and the alumina-magnesia refractory.
2. The relationship between the initial contact angle and selenium content in iron was calculated, agreeing well with the measured results. The calculation can be used to predict the wettability between Fe-Se alloy and refractory.
3. The liquid iron penetrated into the refractory through pores. The liquid iron in pores can prevent the further penetration of the liquid iron. The liquid iron penetration depth decreased with the addition of selenium in iron.

ACKNOWLEDGMENTS

The authors are grateful for the support from the National Science Foundation of China (Grant No. U1860206) and the Fundamental Research Funds for the Central Universities (Grant No. FRF-TP-17-001C2). The Beijing Key Laboratory of Green Recycling and Extraction of Metals (GREM), the Laboratory of Green Process Metallurgy and Modeling (GPM^2), and the High Quality Steel Consortium (HQSC) at the School of Metallurgical and Ecological Engineering at the University of Science and Technology Beijing (USTB) are also acknowledged.

REFERENCES

1. A.M. Garbers-Craig: *J. S. Afr. Inst. Min. Metall.*, 2008, vol. 108, pp. 1–16.
2. L. Zhang and B.G. Thomas: *ISIJ Int.*, 2003, vol. 43, pp. 271–91.
3. X. Zou, D. Zhao, J. Sun, C. Wang, and H. Matsuura: *Metall. Mater. Trans. B*, 2018, vol. 49B, pp. 481–89.
4. F.L. Riley: *Key Eng. Mater.*, 1996, vol. 113, pp. 1–14.
5. J. Křesťan, O. Pritula, L'. Smrčok, P. Šajgalík, Z. Lenčéš, A. Wannberg, and F. Monteverde: *J. Eur. Ceram. Soc.*, 2007, vol. 27, pp. 2137–43.
6. I.U.H. Muhammad, R. Khanna, P. Koshy, and V. Sahajwalla: *ISIJ Int.*, 2010, vol. 50, pp. 804–12.
7. X.J. Zhao, H.Q. Ru, N. Zhang, X.Y. Wang, and D.L. Chen: *Ceram. Int.*, 2013, vol. 39, pp. 3049–54.
8. P. Shen, L. Zhang, and Y. Wang: *Metall. Res. Technol.*, 2016, vol. 113, p. 503.
9. A. Huang, Y. Wang, Y. Zou, H. Gu, and L. Fu: *Ceram. Int.*, 2018, vol. 44, pp. 14617–24.
10. Y. Wei, Y. Shao, J. Chen, and N. Li: *J. Eur. Ceram. Soc.*, 2018, vol. 38, pp. 313–22.
11. J. Fruhstorfer, L. Schöttler, S. Dudczig, G. Schmidt, P. Gehre, and C.G. Aneziris: *J. Eur. Ceram. Soc.*, 2016, vol. 36, pp. 1299–1306.
12. A. Zhukovskaya, E. Sherman, E. Prokofeva, and T. Korableva: *Refractory*, 1982, vol. 23, pp. 504–07.
13. K. Ogino, K. Nogi, and O. Yamase: *ISIJ Int.*, 1983, vol. 23, pp. 234–39.
14. K. Nogi and K. Ogino: *Can. Metall. Q.*, 2013, vol. 22, pp. 19–28.
15. A.Y. Zaslavskii, Y.E. Goldshtein, and R. Shenk: *Met. Sci. Heat Treat.*, 1967, vol. 9, pp. 694–96.
16. M.W. George: *Minerals Yearbook,* Bureau of Mines, U.S. Government Printing Office, Washington, DC, 2003, pp. 65.1–65.8.
17. D.S. Petrovič: *ISIJ Int.*, 2011, vol. 51, pp. 1539–44.
18. J. Tanabe: *Steel Res. Int.*, 2006, vol. 77, pp. 21–24.
19. M.R. Aboutalebi, M. Isac, and R.I. Guthrie: *Steel Res. Int.*, 2004, vol. 75, pp. 366–72.
20. M. Jenko, J. Fine, and D. Mandrino: *Surf. Interface Anal.*, 2000, vol. 30, pp. 350–53.
21. V.C. Schwindt, J. Ardenghi, P. Bechthold, E. González, P. Jasen, A. Juan, B. Batic, and M. Jenko: *Appl. Surf. Sci.*, 2014, vol. 315, pp. 252–60.
22. P. Sahoo, T. Debroy, and M.J. Mcnallan: *Metall. Mater. Trans. B*, 1988, vol. 19B, pp. 483–91.
23. T. Yoon, K. Lee, B. Lee, and Y. Chung: *ISIJ Int.*, 2017, vol. 57, pp. 1327–33.
24. S. Ueda, S. Suzuki, T. Yoshikawa, and K. Morita: *ISIJ Int.*, 2017, vol. 57, pp. 97–403.
25. H. Choi and H. Liang: *J. Colloids Interface Sci.*, 2016, vol. 477, pp. 176–80.
26. A. Marmur: *Adv. Colloids Interface Sci.*, 1992, vol. 39, pp. 13–33.
27. P. Yue and Y. Renardy: *Phys. Fluids*, 2013, vol. 25, p. 052104.
28. Y. Yu, X. Wang, and T.W. Ng: *J. Colloids Interface Sci.*, 2012, vol. 376, pp. 269–73.

Publisher's Note Springer Nature remains neutral with regard to jurisdictional claims in published maps and institutional affiliations.